SLAC-PUB-6161
SLAC/SSRL-0026
April 1993
(SSRL/ACD)

Simple Approximations To Transverse Wiggler Spectra Integrated Over Finite Apertures In the Wiggle Plane*

Roman Tatchyn

Stanford Linear Accelerator Center
Stanford Synchroton Radiation Laboratory
Stanford University, Stanford, CA 94309

Abstract

Simple approximations to conventional transverse wiggler spectra integrated over finite apertures in the wiggle plane are derived. Account is taken of the departure of the wiggler's on-axis field profile from an idealized sinusoidal shape. By introducing a generalization of the conventional K parameter, it is shown that the approximations can be formulated from a Fourier decomposition of the wiggler's dominant field profile in the direction of particle motion without explicit reference to the particle beam trajectory. Use of the generalized K parameter for estimating the first harmonic output energies of undulators and the critical energies of wigglers is examined.

Submitted to *Nuclear Instruments and Methods*

*Work supported in part by the Department of Energy contract DE-AC03-76SF00515 and DOE Offices of Basic Energy Sciences and High Energy and Nuclear Physics.

1. Introduction

Conventional studies of transverse insertion devices, in particular undulators and wigglers, rely heavily on the so-called "deflection parameter" K ($K=0.934B_M[T]\lambda_w[cm]$, where B_M is the peak on-axis field and λ_w is the device period) to arrive at simplified expressions for their basic spectral output parameters [1,2]. As will be shown below, however, this practice is strictly justified only when the transverse (i.e., dominant) field component in the direction of motion is purely sinusoidal. Thus, when calculating the spectral performance of structures in which the field can be appreciably non-sinusoidal, care must be taken to reassess the validity of K.

In this note our primary focus will be on deriving approximations to selected spectral properties of transverse wigglers, devices which, in conventional parlance, have a "high" value of K (conventionally, $K \geq 10$ [2]). Specifically, we will be interested in the spectral intensity distribution of wiggler radiation fully integrated in a direction perpendicular to the wiggle plane and integrated over a finite angular aperture in the wiggle plane. As will be shown, the departure of a wiggler's field profile from a purely sinusoidal shape can be an important determinant of its spectral properties, and a suitable generalization of K will be required to help parametrize expressions describing the integrated angular and spectral characteristics of its radiation. To minimize complications, we will restrict our analysis to field profiles that: 1) are

symmetric and have a single maximum (or minimum) within each half-period; 2) attain their maximum slopes at points where the field changes sign; and 3) increase or decrease monotonically between zero and the extremum within each half period.

2. Fully angle-integrated wiggler spectra

A schematic of the geometric parameters relevant to our study is shown in Fig. 1. The wiggler structure is taken to consist of N periods (2N poles), and the K parameter is assumed to be large enough to inhibit coherence effects among the individual poles. In this regime, the radiation generated by an incremental arc of trajectory can be approximated by the radiation along an instantaneously circular arc with a matching radius of curvature. The total spectral-angular intensity distribution of this radiation, expressions for which are derived in Jackson [3], can consequently be obtained by linearly adding the incremental spectral-angular distributions associated with each arc over the entire length of wiggler. For N substantially large, all the periods substantially similar, and the point of observation sufficiently far away, the additions need be performed over only one half period and the result multiplied by 2N. We note that the wiggler trajectory (and particle energy) naturally defines the angular limits of its radiation (viz., to within an angular interval of $+2/\gamma$, where $\gamma = E/mc^2$, m is the particle mass, c is the velocity of light, and E is the particle energy). For γ

sufficiently large, the full angular interval in the far field associated with the depicted trajectory is seen to be approximately $2\theta_M$, where

$$\theta_M \approx \left| \left(\frac{dx}{dz}\right)_{(z=0,\pm\lambda_u/2,\ldots)} \right|. \qquad (1)$$

The quantity in absolute value brackets is the slope of the trajectory at its intersection points with the z axis.

Our starting point will be the angle-integrated expression for the spectral radiated-energy distribution of an electron on a circular trajectory derived in [3], viz.,

$$\left(\frac{dE}{d\omega}\right) \text{[ergs/electron,revolution,unit frequency interval]} \approx$$

$$\sqrt{3}\,\frac{e^2\gamma\omega}{c\omega'_c}\int_{\omega/\omega'_c}^{\infty} K_{5/3}(y')\,dy'. \qquad (2)$$

The constants in eq. (2) are in CGS units, with $\omega'_c=\omega_c/2$, where ω_c, the "critical frequency," is given by $3\gamma^3 c/\rho$ [3], and ρ, expressed as

$$\rho\,[\text{cm}] = 335E[\text{GeV}]/B[\text{T}], \qquad (3)$$

is the radius of curvature. B is the field seen by the elecron, and $K_{5/3}(y')$ is a modified Bessel function of the second kind.

Converting (in MKS) from ergs per electron to photons per second, from frequency to photon energy (in keV), and converting to "per horizontal milliradian" units in the wiggle plane, we arrive at the following expression [2] for the spectral-angular distribution of Φ, the photon flux per 0.1% bandwidth per second, generated by a circular trajectory, viz.,

$$\left(\frac{d\Phi}{d\theta}\right)[\text{ph/s,mr,0.1\%BW}] \approx 2.457\times10^{10}E[\text{GeV}]I[\text{mA}]\frac{\varepsilon}{\varepsilon_c}\int_{\varepsilon/\varepsilon_c}^{\infty}K_{5/3}(y')dy'. \quad (4)$$

Here ε_c, the "critical energy," is given by $10^{-3}\omega_c'h[\text{J-s}]/2\pi q[\text{C}]$; h and q are, respectively, Planck's constant and electronic charge; and I is the particle beam current.

To obtain the total distribution angle-integrated in the wiggle plane over one wiggler pole, we can now evaluate eq. (3) at each point on the trajectory (viz., as a function of z) and multiply it by the local angular arc $d\theta$. Due to the smallness of the trajectory excursion for ultrarelativistic electrons and realistic wiggler parameters, the arc length of the trajectory over one half period will, to second order, be equal to $\lambda_w/2$, and we can consequently utilize the approximation $d\theta \approx dz/\rho(z)$. Thus,

$$\langle\Phi(\varepsilon)\rangle_{2\theta_M}[\text{ph/s,0.1\%BW}] \approx 1.1\times10^{13}\frac{I\varepsilon}{E^2}\int_0^{\lambda_w/2}dz\int_{\varepsilon/\varepsilon_c(z)}^{\infty}K_{5/3}(y')dy'. \quad (5)$$

As is evident, the total angle-integrated flux is now an implicit function of the profile of the dominant field component B(z) (via $\varepsilon_c(z)=0.665E^2B(z)$) in the lower limit on the rightmost integral in eq. (5). The complete flux distribution in the far field, integrated over the above limits, is then given by

$$\Phi(\varepsilon)\,[\mathrm{ph/s,0.1\%BW}] \approx 2N\langle\Phi(\varepsilon)\rangle_{2\theta_M}. \qquad (6)$$

We can now examine the effect of the field profile B(z) on $\Phi(\varepsilon)$. For maximum contrast we will compare the effect of a sinusoidal-field half-period vs. a constant-field half-period. The former profile is typical of many existing insertion devices, while a physical approximation to the latter could be generated by, e.g., full periods composed of two contiguous and alternating permanent magnet pairs with a gap $\ll \lambda_w$. For both structures we assume the parameters of the Beam Line 10 wiggler on SPEAR, viz., I=100 mA, E=3 GeV, N=15, λ_w=12.85cm, and B_0=1.45T. Thus, the field in the first case can be expressed as $B(z)\approx 1.45\sin(2\pi z/\lambda_w)$, and by $B(z)\approx 1.45$ in the second case. We note that in both cases the conventional definition of the deflection parameter yields a K value of approximately 17.4.

The results of both calculations are plotted on log-log and log-lin axes in Fig. 2. As is intuitively plausible, the constant-field half-period is seen to generate substantially more power relative to the sinusoidal half-period, particularly in the regions at and to the right of the curves' maxima. The effective critical energy of the sinusoidal half-period is also seen to be

effectively shifted to a lower value than the constant-field device. The depicted curves clearly underscore the conditional utility of K for determining the spectral properties of arbitrarily-defined insertion devices.

3. Wiggler spectra integrated over finite wiggler-plane apertures

We now turn to the calculation of wiggler spectra integrated over finite apertures in the wiggle plane. Referring to Fig. 1, it is evident that every aperture bounded by $2\theta_M$ will define two tangent points (L,R) on the wiggler trajectory. These two points in turn define an interval $[Z_L, Z_R]$ along z which is seen to lie between the end-point of the wiggler's half-period interval $[0,\lambda_w/2]$. To calculate the contribution from each wiggler pole to the flux collected by the aperture, the procedure is, evidently, to change the integration limits in the outside integral on the right hand side of eq. (5) from $[0,\lambda_w/2]$ to $[Z_L, Z_R]$.

To perform the indicated procedure, it is apparent that the slope of the trajectory vs. z is required to find the two tangent points associated with a selected aperture and to identify the corresponding points Z_R and Z_L. For the limiting cases $Z_R=0$ and $Z_L=\lambda_w/2$, it is evident from eq. (1) that the slope is also required to define the maximum aperture $2\theta_M$. To find the desired expression for the trajectory slope, then, we first turn to the equations of motion of an (ultrarelativistic) electron in the wiggler field.

Assuming a sufficiently long wiggler with sufficiently wide pole faces, we first approximate the dominant field component (taken parallel to the y axis) in the vicinity of the z axis by its Fourier series expansion, viz.,

$$B(z) \approx \sum_{n=0}^{\infty} B_n \sin(2\pi z/\lambda_n) \ , \tag{7}$$

with

$$\lambda_n = \lambda_w/(1+n) \ . \tag{8}$$

Then, the desired equations of motion are:

$$\gamma m\dot{x} = -q\dot{z} \sum_{n=0}^{\infty} B_n \sin(2\pi z/\lambda_n) \ , \tag{9}$$

and

$$\gamma m\dot{z} = q\dot{x} \sum_{n=0}^{\infty} B_n \sin(2\pi z/\lambda_n) \ . \tag{10}$$

The solutions for the x and z components of velocity (assuming standard initial conditions) can be written down by inspection, viz.,

$$\dot{x} = -\frac{q}{\gamma m 2\pi} \sum_{n=0}^{\infty} \lambda_n B_n \cos(2\pi z/\lambda_n) \ , \tag{11}$$

and

$$\dot{z} = \left(\beta^2 c^2 - \left[\frac{q}{\gamma m 2\pi} \sum_{n=0}^{\infty} \lambda_n B_n \cos(2\pi z/\lambda_n) \right]^2 \right)^{1/2} \ , \tag{12}$$

where βc is the particle's speed outside of the wiggler, and $\beta^2 = 1 - \gamma^{-2}$.

We now introduce a generalized deflection parameter K_n, where

$$K_n = \frac{q\lambda_n B_n}{2\pi m\beta c} \approx 0.934\lambda_n[\mathrm{cm}]B_n[\mathrm{T}], \tag{13}$$

and a generalized "deflection angle" δ_n^w, where

$$\delta_n^w = K_n/\gamma . \tag{14}$$

Associated with these will be the total deflection and total deflection angle parameters K_T and δ_T^w, where

$$K_T = \sum_{n=0}^{\infty} K_n, \tag{15}$$

and

$$\delta_T^w = \frac{K_T}{\gamma} . \tag{16}$$

Using equs. (11) and (12), we can now straightforwardly express the desired trajectory slope dx/dz as a function of z and the generalized deflection angles δ_n^w,

$$\frac{dx}{dz} = \frac{\sum_{n=0}^{\infty} \delta_n^w \cos(2\pi z/\lambda_n)}{\left\{1 - \left(\sum_{n=0}^{\infty} \delta_n^w \cos(2\pi z/\lambda_n)\right)^2\right\}^{1/2}}. \tag{17}$$

Clearly, eq. (17) defines the desired trajectory slope vs. z without explicit reference to the trajectory. All that is required is a Fourier decomposition of the wiggler field profile

vs. z.

Setting z=0 in eq. (17), we can now simply express the maximum trajectory angle θ_M of eq. (1) by

$$\theta_M \approx \frac{K_T}{\gamma}\left(1 - \left(\frac{K_T}{\gamma}\right)^2\right)^{-\frac{1}{2}}. \qquad (18)$$

Of interest for many calculations is the average velocity of progression of the particle in the z direction through the wiggler field. Assuming $\delta_T^w \ll 1$, we can expand and average eq. (12) over the interval $[0,\lambda_w]$ to obtain

$$\langle \dot{z} \rangle_{WIGGLER} = \beta^* c \approx \beta c \left\{1 - \frac{1}{4}\sum_{n=0}^{\infty}\left(\frac{K_n}{\gamma}\right)^2 + \ldots\right\}. \qquad (19)$$

For a purely sinusoidal field, i.e., $B_n=0$ (i=1,2,3,...), both equs. (18) and (19) (together with (9) and (10)) can be seen to assume interpretations consistent with the conventional definition of K.

4. General computational procedure

For practical purposes, it will be convenient to summarize the assumptions and steps associated with calculating a realistic wiggler spectrum for a given aperture. In addition to the restriction that γ^{-1} be sufficiently smaller than the angular aperture in question, a similar constraint will be applicable to the component of angular divergence in the wiggle plane contributed by the particle beam emittance Σ and the lattice beta

function β_w at the wiggler location. Thus, apart from the underlying assumption that the insertion device in question is operating substantially in the wiggler regime, the basic conditions for applying the computational scheme outlined in this note can be summarized as follows:

a) $((\Sigma/\beta_w)+\gamma^{-2})^{1/2} \ll (\theta_L-\theta_R)$;

b) the entire wiggler radiation fan is assumed to be collected by the aperture in the direction perpendicular to the wiggle plane;

c) N is assumed to be sufficiently large for a sufficiently accurate representation of the wiggler field by a Fourier series expansion. If N is too small (as might be the case, for example, for a wavelength shifter), decomposition of the field by Fourier transforms must be employed, and the series expansions in equs. (7), (9-12), (15), (17), and (19) must be generalized to the appropriate integral forms.

The following sequence of computational steps can be followed:

1) obtain the functional profile of the wiggler field (this can be extracted from field measurement data, or from approximate calculations based on fitting structural and magnetic-parameter information to suitable simulation models.

2) perform a Fourier series decomposition of the field choosing the point in the center of the wiggler where the field changes sign as origin.

3) using a sufficient number of the derived Fourier coefficients, calculate K_T via equs. (13) and (15) and the trajectory slope vs. z via eq. (17).

4) determine the maximal angular aperture $2\theta_M$ via eq. (18).

5) define the desired observation aperture in the far field by selecting θ_L and θ_R, verifying that the angular aperture $(\theta_L - \theta_R)$ falls within $2\theta_M$. Subject to this constraint, it should be noted that the selected aperture need not be centered on the z axis, but can be asymmetrically located, including entirely off the wiggler axis.

6) using the calculated trajectory slope vs. z, find the z-locations (i.e., z_L and z_R) of the tangent points L and R defined by the limit angles θ_L and θ_R of the selected aperture.

7) perform the desired calculation using equs. (5) and (6) with suitably modified integration limits.

Should the aperture be too close to the wiggler for the straightforward application of equs. (5) and (6) to apply, an evident modification of the above procedure would be to first use the aperture dimensions and distance from the wiggler to identify the correct trajectory tangent points for each individual pole, and then integrate with eq. (5) between the corresponding limits along the z axis for each pole.

5. Discussion

We have developed a computational procedure, based on a generalization of the conventional deflection parameter K, for calculating wiggler spectra integrated over finite apertures in the wiggle plane. The significant difference found between typical spectra generated by a sinusoidal vs. flat field profiles raises the general question of how higher field harmonics can influence the standard spectral parameters of insertion devices with arbitrary values of K, and whether the generalized K introduced in this paper could be used to account for this influence.

To query this, we will briefly consider a generalized definition of a wiggler's critical energy, ε_c, and the standard definition of an undulator's first harmonic photon energy, ε_1. Appealing to arguments used in deriving eq. (5), ε_c can be defined for a given field profile as

$$\varepsilon_c = \frac{\int_0^{\lambda_w/2} dz \left(\frac{\varepsilon_c(z)}{\rho(z)}\right)}{\int_0^{\lambda_w/2} \rho(z)^{-1} dz.} = .665E^2 \frac{\int_0^{\lambda_w/2} B(z)^2 dz}{\int_0^{\lambda_w/2} B(z) dz.} . \qquad (20)$$

The maximum ε_c evidently occurs for a flat-field trajectory, which can be used as a convenient referent.

For the undulator, ε_1 in the forward direction can be expressed as [4]

$$\varepsilon_1 \approx 0.949E^2/\lambda_u(1-\beta^*), \qquad (21)$$

where $\beta^* c$ is the average forward velocity of the particle beam through the undulator field.

To investigate these two parameters numerically, we will utilize the two trajectories shown in Fig. 3. The Fourier series representation of the rightmost one is simply $B_0 \sin(2\pi z/\lambda_0)$, with $B_0 = B_M$. Clearly, $K_T = K$. The coefficients in the expansion of the leftmost trajectory are straightforwardly derived to be

$$B_n = \frac{2\lambda_w B_M}{(n+1)^2 \pi^2 e} \sin\left(\frac{2\pi(n+1)e}{\lambda_w}\right) ; \qquad n=0,2,4,... \tag{21}$$

Choosing $e = \lambda_{w(u)}/8$, we find $K_T \approx 1.18K$. To determine ε_1 for an undulator, we insert the result of eq. (19) into eq. (21) to yield

$$\varepsilon_1 \approx 0.949(E^2/\lambda_{w(u)}) \left\{1 + \frac{1}{2}\sum_{n=0}^{\infty} K_n^2 + \ldots\right\}^{-1}. \tag{22}$$

Clearly, for the sinusoidal trajectory the expression in brackets on the right hand side becomes the familiar $(1+0.5K^2)$. For the trapezoidal trajectory, performing the indicated summation yields the increased value $(1+0.658K^2)$.

To derive ε_c for the trajectories in the high-K (wiggler) case, we first note that the numerator, by Parseval's identity, is just equal to one half of the infinite summation of the squares of the coefficients B_n, while each term of the integrated series in the denominator is given simply by

$$\frac{2}{\lambda_w}\int_0^{\lambda_w/2} B_n \sin\left(\frac{2\pi(n+1)z}{\lambda_w}\right) dz = \frac{2}{\pi(n+1)} B_n. \tag{23}$$

Thus, for the sinusoidal trajectory we have $n=0$, $B_0=B_M$, and the critical energy for the sine-field wiggler will be given by $\varepsilon_{c(sine)}=\pi\varepsilon_{c(flat)}/4$ (see Fig. 2). For the trapezoidal trajectory (with $e=\lambda_w/8$), the corresponding calculations lead to $\varepsilon_{c(trap.)}=0.89\varepsilon_{c(flat)}$.

In Table 1. we plot these results for three different devices spanning a typical range of field strengths and periods. It is evident that in both the wiggler and undulator regimes serious mis-estimates of the 1st harmonic energy of an undulator or the critical energy of a wiggler can result if the detailed harmonic composition of the insertion device field is not taken into account.

Before concluding our note, we can pause to evaluate some of the physical and mathematical implications of our analysis. We first note that in our generalization of K we have in fact invoked more than one new parameter. Thus, we have utilized the indexed K_n (and B_n) as well as functions (such as the sums of K_n and K_n^2 over n) defined on them. Physically, this corresponds to the circumstance that an arbitrary periodic field and its effect on the radiated spectrum does, in general, require a parameter set containing more than one element for a physically complete description. In the present analysis we have chosen this set to be the coefficients associated either with the Fourier expansions of B(z) or the x-component of the particle velocity. We have also demonstrated that more than one function useful for parametrizing spectral parameters can be associated with the coefficient sets. For each field profile B(z), then, the generalized K introduced in

this note can be conveniently viewed as the pair of sets $\{\kappa=\{K_0,K_1,.....\},\kappa_K\}$, where κ_K is the set of applicable functions defined on κ. Similarly, the same association can be made for for the set of field coefficients B_n. From this perspective the status of the conventional definition and usage of K, viz., for arbitrary transverse insertion devices, can be seen to be physically justified only when the Fourier coefficient sets contain the single elements K_0 (and B_0). The same analytical criteria and comments are also applicable to insertion device structures (e.g., helical) for which the Fourier decomposition of more than one field component is required.

Together with the extension of the single parameters K and B_M to multi-element sets, it appears evident that additional interesting directions for further work are suggested by the present study. For example, the identification of additional functions composed from the coefficient sets that could be used to describe the physical and spectral properties of arbitrary insertion devices more economically would be important. For example, the conventional distinction drawn between an undulator and a wiggler implies that for intermediate values of K a description based solely on ε_c or ε_1 will be incomplete. A second related issue, appropriate to on-axis apertures, is the emission of undulator-like radiation by a wiggler from the low-field portions of its trajectory. For an intermediate-K device, the undulator portion would still constitute a significant portion of the total radiation, and would be important in determining not only the angle-integrated, but the angle-dependent spectral

distributions in the observation plane. For addressing these issues, especially for devices with harmonically complex periodic fields, it seems apparent that analysis based on the Fourier components of the field, applied both in the laboratory and moving electron frames [5], is an appropriate direction for further investigations.

6. Acknowledgements

The initial suggestion for this study by Herman Winick is acknowledged. This research was performed at SSRL which is operated by the Department of Energy, Office of Basic Energy Sciences, Division of Chemical Sciences. That Office's Division of Materials Sciences has provided support for this research.

Table 1.

Selected spectral parameters of undulators and wigglers calculated with the conventional vs. generalized deflection parameters for sinusoidal (sine) vs. trapezoidal (trap.) field profiles. E=3GeV.The slopes of the trapezoid inclines are $\pm 8B_M/\lambda_{w(u)}$. The conventional criterion ($K \geq 10$) for defining a wiggler is utilized.

	B_M=0.3T; λ_u=6cm (undulator)		B_M=1T; λ_u=3cm (undulator)		B_M=1.5T; λ_w=16cm (wiggler)	
	sine	trap.	sine	trap.	sine	trap.
K	1.68	1.68	2.8	2.8	22.4	22.4
K_T	1.68	1.98	2.8	3.3	22.4	26.4
$\varepsilon_1(K)$	0.59	0.59	0.58	0.58	-	-
$\varepsilon_1(K_T)$	0.59	0.50	0.58	0.46	-	-
$\varepsilon_c(K)$	-	-	-	-	9	9
$\varepsilon_c(K_T)$	-	-	-	-	7.07	8

7. References

[1] S. Krinsky, T. L. Perlman, and R. E. Watson, "Characteristics of Synchrotron Radiation and of Its Sources," in Handbook on Synchrotron Radiation, ed. E. E. Koch, North-Holland Physics Publishing, Amsterdam, 1983, pp. 65-171.

[2] K.-J. Kim, "Characteristics of Synchrotron Radiation," in X-Ray Data Booklet, Douglas Vaughan, ed., Lawrence Berkeley Laboratory PUB-490 Rev., 1986, p. 4-1.

[3] J. D. Jackson, Classical Electrodynamics, John Wiley and Sons, New York, 1975, pp. 672-679.

[4] R. Coisson and R. Tatchyn, "Introduction to Optical Properties of Insertion Devices Excited by Synchrotron Sources," in Tutorial T1, International Conference on Insertion Devices for Synchrotron Sources, SSRL, Stanford University, October 27, 1985, SPIE Proceedings No. 582, 1986.

[5] R. Tatchyn and I. Lindau, "Off-axis radial properties of undulator light," SPIE Proceedings No. 733, 115(1987).

Figure Captions

Figure 1. Schematic top views of a wiggler particle trajectory in the wiggle plane. The limiting angle of observation, $2\theta_M$, is defined by the trajectory slope at its crossing points with the z axis. The arbitrary angle of observation $(\theta_R - \theta_L)$ defines the z-axis points Z_L and Z_R via the tangent points L and R on the trajectory. It is assumed that the natural divergence angle γ^{-1} associated with each source point of the trajectory fulfills the condition $\gamma^{-1} \ll (\theta_R - \theta_L)$. Observation distances and angles are not to scale.

Figure 2. Wiggler spectra for two devices with the same nominal parameters but with flat vs. sinusoidal field distributions within each half-period. Both log-log (top) and log-lin (bottom) representations are shown.

Figure 3. Two field profiles for assessing the use of the generalized deflection parameter for describing the spectral properties of emitted radiation. The rightmost field profile is purely sinusoidal. The leftmost profile, while non-physical, can be viewed as a simplified limit to which real insertion devices with small gap/period ratios can approximate.

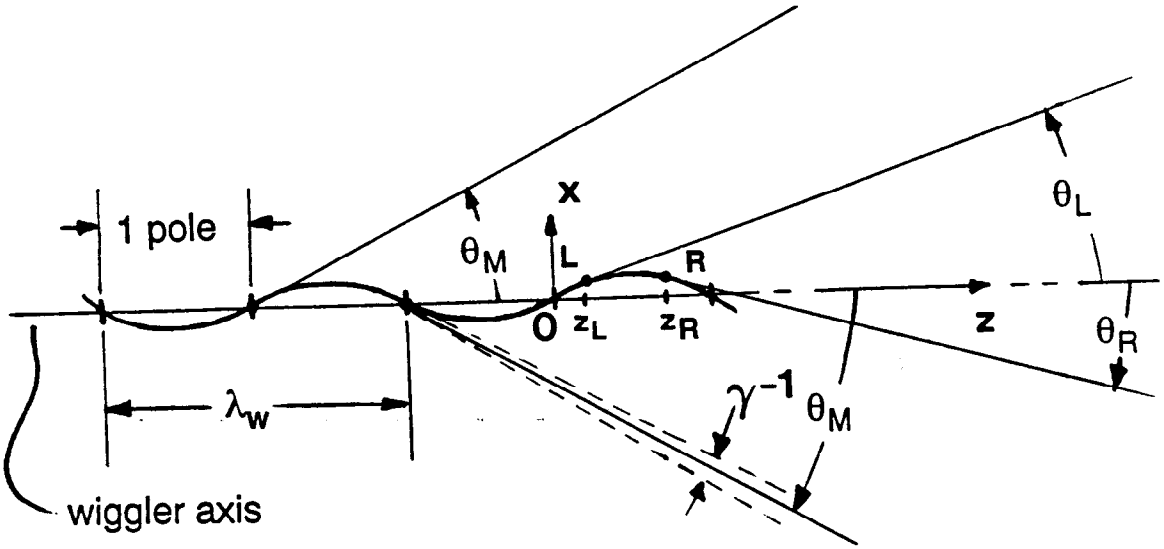
1 pole
θ_M
X
L
R
O
z_L
z_R
θ_L
Z
θ_R
λ_w
γ^{-1}
θ_M
wiggler axis

FIG. 1

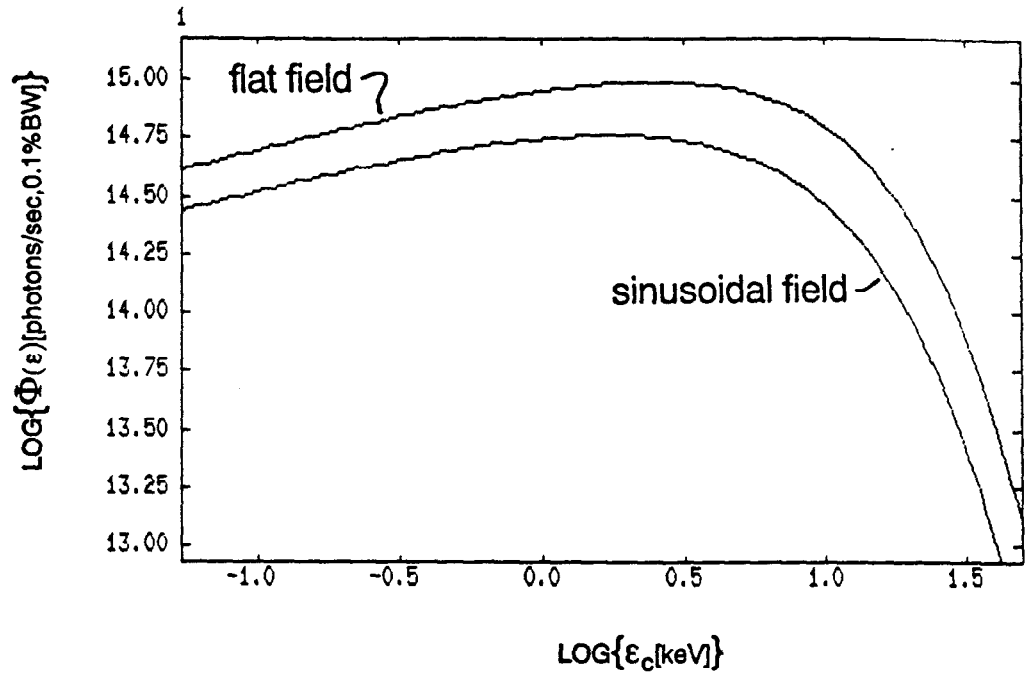
1
15.00
14.75
14.50
14.25
14.00
13.75
13.50
13.25
13.00
flat field
sinusoidal field
LOG{Φ(ε)[photons/sec,0.1%BW]}
-1.0
-0.5
0.0
0.5
1.0
1.5
LOG{εc[keV]}

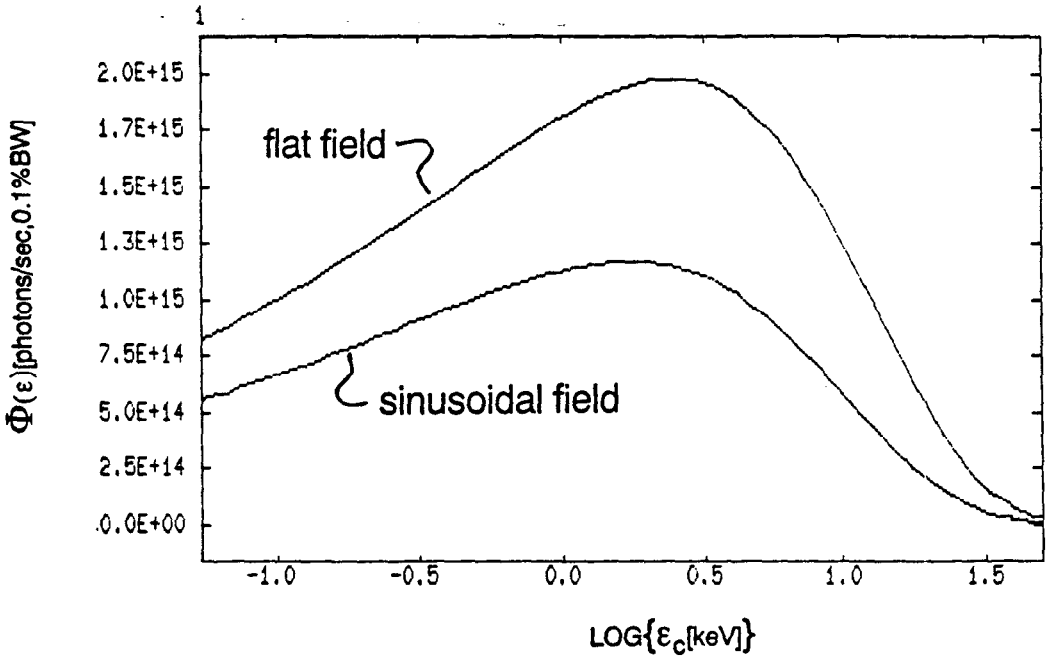
1
2.0E+15
1.7E+15
1.5E+15
1.3E+15
1.0E+15
7.5E+14
5.0E+14
2.5E+14
.0.0E+00
flat field
sinusoidal field
Φ(ε)[photons/sec,0.1%BW]
-1.0
-0.5
0.0
0.5
1.0
1.5
LOG{εc[keV]}

FIG. 2

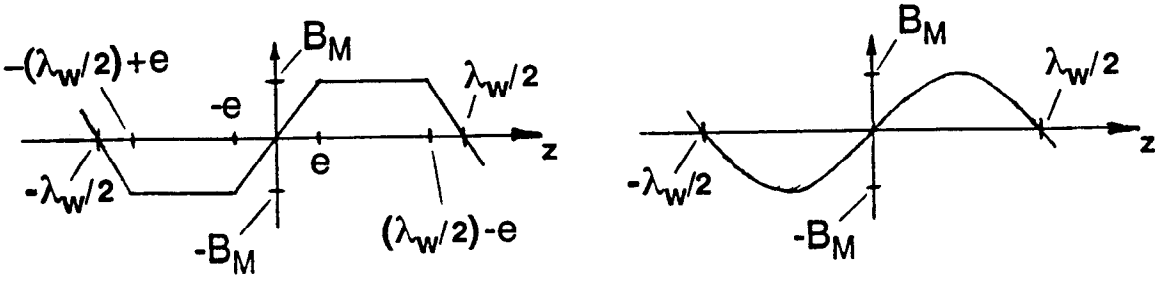
B_M
$-(\lambda_w/2)+e$
$-e$
$\lambda_w/2$
z
e
$-\lambda_w/2$
$-B_M$
$(\lambda_w/2)-e$
B_M
$\lambda_w/2$
z
$-\lambda_w/2$
$-B_M$

FIG. 3